

**Paper-based device of designer soft layered polymer composites for measurement of weak friction force**

Journal:	<i>Journal of Materials Chemistry C</i>
Manuscript ID	TC-ART-10-2019-005396.R1
Article Type:	Paper
Date Submitted by the Author:	09-Nov-2019
Complete List of Authors:	Watanabe, Kei; Keio University, Department of Applied Chemistry, Faculty of Science and Technology Imai, Hiroaki; Keio University, Department of Applied Chemistry, Faculty of Science and Technology Oaki, Yuya; Keio University, Department of Applied Chemistry, Faculty of Science and Technology

ARTICLE

Paper-based device of designer soft layered polymer composites for measurement of weak friction force

Kei Watanabe,^a Hiroaki Imai,^a Yuya Oaki^{*,a,b}

Received 00th January 20xx,
Accepted 00th January 20xx

DOI: 10.1039/x0xx00000x

Measurement of friction force is important for safety, security, and health of our life. Excessive friction force causes degradation of materials and biological bodies. For example, tooth enamel and gum are damaged by strong toothbrushing force. However, friction force is not easily measured by conventional materials and devices. Here we proposed the design strategies of paper-based device for measurement of friction force. Toothbrushing force, a model of weak friction force, is the measurement target in the present work. The soft layered composites of polydiacetylene (PDA) and interlayer guest macromolecule were designed and synthesized to achieve visible color change in response to weak friction force. A data-scientific approach assisted selection of the interlayer guest molecule to control the stimuli responsivity of the layered PDA. The guest polyethyleneimine (PEI) formed the soft layered composites exhibiting the color change in response to weak friction force. The paper-based device of the layered PDA/PEI composite showed the gradual color change from blue to red in response to the strength and number of the applied friction force. As a model case, toothbrushing force was measured using the paper-based device. The present work shows new design strategies of molecules and materials toward measurement of a wide variety of friction force.

Introduction

Mechanical stress, such as shear, compression, and tensile stresses, causes degradation and damage of materials. Materials and devices for detection of mechanical stresses are required to alert before serious damages. Mechano-responsive materials have been rapidly developed for visualization and detection of mechanical stresses.^{1–5} Mechano-responsive materials have potentials for application to wearable and biocompatible sensing devices.^{6–8} Mechanical stresses are detected by changes of visible and/or fluorescent colors through the structure transition of materials containing chromophores.^{9–21} Compression and tensile stresses with macroscopic deformation were visualized and quantified using stimuli-responsive soft materials.^{9–15} Although friction force was visualized by changes of fluorescent color,^{16–21} the quantification is still an important challenge in materials science. In general, the strength and number of the applied friction force are not easily quantified by the color because the original color turns at certain threshold with the structure transition. If the color is gradually changed in response to strength and number of the applied friction force, not only the visualization but also the quantitative measurement can be achieved by the color. A number of health problems, such as

bedsores and thrombus, are related to shear stress.^{22–26} For example, toothbrushing force has attracted interests.^{25,26} Although the strength is represented by force normal to teeth,^{27,28} the brushing force is not quantified as friction force. Therefore, new materials and devices with tunable stimuli responsivity are required for measurement of a wide range of friction force. Here we propose the design strategies of materials and devices for measurement of friction force. Paper-based device of designer soft layered polydiacetylene (PDA) enables measurement of toothbrushing force as a model of weak friction force (Fig. 1).

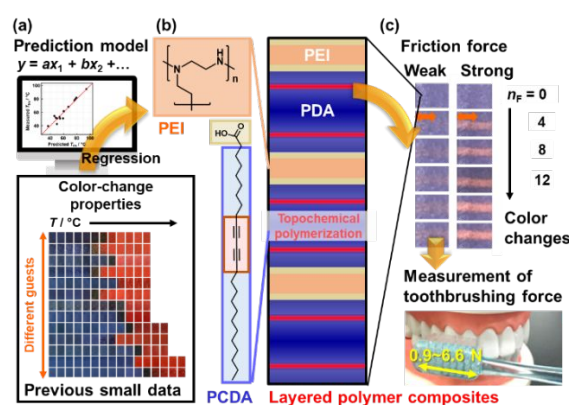


Fig. 1 Design strategies of materials and devices for measurement of friction force using layered polymer composites of PDA and PEI. (a) Sparse modeling toward prediction of the stimuli-responsive color-change properties using previous our experimental data. (b) Layered composites of PCDA and PEI synthesized by self-organization and their topochemical polymerization to PDA/PEI. (c) Visualization of the applied friction on the PDA/PEI paper-based device and its application to measurement of toothbrushing force.

^a Department of Applied Chemistry, Faculty of Science and Technology, Keio University, 3-14-1 Hiyoshi, Kohoku-ku, Yokohama 223-8522, Japan

^b JST, PRESTO, 4-1-8 Honcho, Kawaguchi 332-0012, Japan

† Email oakiyuya@appc.keio.ac.jp

Electronic Supplementary Information (ESI) available: [Experimental methods, Structure characterization and stimuli responsivity of the reference samples]. See DOI: 10.1039/x0xx00000x

PDA derivatives show color changes with application of external stimuli, such as heat, light, and force.^{29–39} Control of stimuli responsivity, i.e. color-change behavior, is an important challenge for a wide range of sensing applications. For example, improvement of the responsivity is required for detection of weaker friction force, such as toothbrushing force. Application of external stimuli induces motion of the side and PDA main chains.^{34,40} The color is changed by shortening of the effective conjugation length with torsion of the PDA main chain. A general approach to control the stimuli responsivity is design and synthesis of diacetylene (DA) monomers.^{41–50} Our group has developed new intercalation approach to control the stimuli responsivity through tuning the flexibility of the layered structures.^{51–56} Since soft layered materials exhibit dynamic functions,^{57–59} tuning the flexibility is a key to control the properties. Amphiphilic DA monomers, such as 10,12-pentacosadiynoic acid (PCDA), form the layered crystal structure (Fig. 1b). The interlayer space accommodates the guest ions and molecules. The types of the guests have effects on the flexibility of the layered structure determining the stimuli-responsive color-change properties, such as color, responsivity, and reversibility.^{51–56} Our recent work showed visualization of stronger shear stress using the layered composite of PDA and organic amines.⁶⁰ However, the color change was not induced by application of weaker friction force related to health care. In addition, the general design strategies of materials and devices were not elucidated for measurement of diverse friction force. In the present study, new guest molecules for control of the stimuli responsivity were explored with assistance of a data-scientific method (Fig. 1a). According to the resultant design strategy, the layered PDA composites with the enhanced sensitivity were prepared to detect weaker friction force. Moreover, the paper-based device realized the gradual color change in response to number and strength of the applied friction force.

In recent materials science, data science has been used to accelerate exploration of new compounds and enhanced performances.^{61–65} Our group has applied sparse modeling, a data scientific method, to small dataset based on our own experimental results.⁶⁵ Sparse modeling, a recent informatics approach, is utilized to construct a prediction model for explanation of whole behavior by a small number of strongly correlated factors, namely descriptors.^{66,67} The approach can accelerate exploration of synthetic processes and discovery of new materials with enhanced properties. In the present work, the descriptors to control the color-change properties of layered PDA were explored in the previous experimental data using sparse modeling (Fig. 1a). According to the results, polyethyleneimine (PEI) was used as the interlayer guest to obtain the more flexible layered structure (Fig. 1b). The layered composites of PDA and PEI (PDA/PEI) actually showed the color change with application to weaker friction force. The PDA/PEI-coated paper device showed the gradual color change with an increase in the number and strength of the applied friction force (Fig. 1c). A weak friction force, namely toothbrushing force, was actually measured by the color of the resultant device.

Results and discussion

Design strategy of the layered PDA with tunable stimuli responsivity

A few factors related to stimuli responsivity of the layered PDA were explored by sparse modeling (Fig. 2). Since the layered PDA shows color change with heating, the stimuli responsivity is quantitatively characterized by the color-change temperature. A variety of layered PDAs with different temperature-responsive color-change properties were prepared by intercalation of guest organic amines in our previous works.^{53,56,60} Here the descriptors to control the color-change temperature were extracted on the basis of our previous data. The contribution of each factor was firstly compared by a multiple regression analysis. Then, a couple of the descriptors were extracted on the basis of chemical perspective. This simple sparse modeling elucidates the important factors to control the stimuli responsivity.

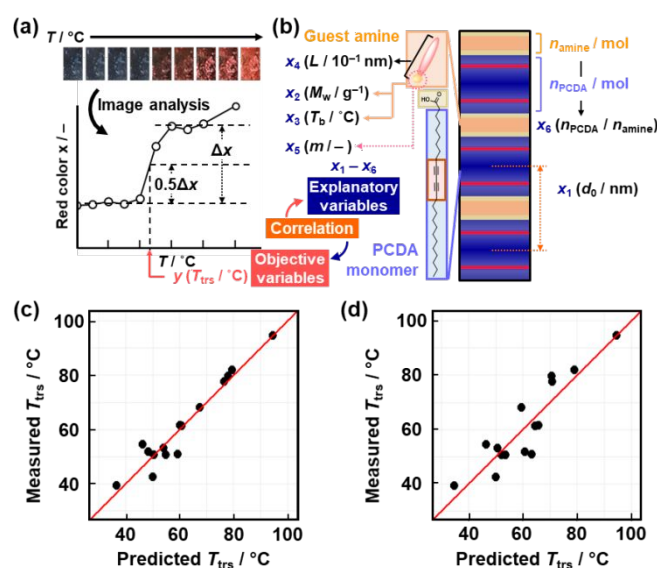


Fig. 2 Sparse modeling toward prediction of T_{trs} . (a) Color-transition temperature (T_{trs}) as an objective variable (y) estimated from the photographs by image analysis. (b) Objective variables (x_i ; $i = 1-6$) related to the layered structures. (c) Relationship between the predicted and measured T_{trs} by the prediction model (eq. 1) using x_1-x_6 . (d) Relationship between the predicted and measured T_{trs} by the prediction model (eq. 2) using the extracted x_1 , x_5 , and x_6 .

Our previous works indicate that the color-change behavior of the layered PDA is characterized by the red-color intensity (x) of the photographs using image analysis, instead of the spectroscopic method (Fig. 2a).^{52,53} In the present work, the simple image analysis was mainly used for characterization of the color-change properties. The x value is estimated from the RGB values of the photographs by image analysis according to an international standard (See Electronic Supplementary Information (ESI)).⁶⁸ The color-transition temperature (T_{trs}) is defined as the temperature to achieve $0.5\Delta x$, where Δx is the increment of the x originating from the color change (Fig. 2a). Whereas the pristine layered PDA showed $T_{\text{trs}} = 64.1$ °C, T_{trs} was changed within 39.2–101.3 °C by the interlayer guest molecules, such as normal alkylamines ($C_n\text{-NH}_2$; $C_n\text{H}_{2n+1}\text{NH}_2$, $n = 1-16, 18$),

normal alkyldiamines ($C_n-(NH_2)_2$: $H_2NC_nH_{2n}NH_2$, $n = 4, 6, 8, 12$), normal dialkylamines ($(C_n)_2-NH$: $H_{2n+1}C_nNHC_nH_{2n+1}$, $n = 4, 6, 8, 10, 12$), and branched alkylamine ($H_{2m+1}C_mCH(NH_2)C_nH_{2n+1}$, $m = 1, n = 5$ and $m, n = 3$).^{53,56,60} The T_{trs} values for the layered PDA samples with 16 different guests were used as objective variables (y) because the data for the following explanatory variables were available (Table S1 in the ESI). The potential factors related to the T_{trs} were set as the explanatory variables (x_i ; $i = 1-6$) (Fig. 2b); the interlayer distance of the layered composite (x_1, d_0), molecular weight of the guest (x_2, M_w), boiling point of the guest (x_3, T_b), molecular length of the guests (x_4, L), the number of the amino groups in the guest molecule (x_5, m), and measured molar ratio of PCDA monomer to the guest amine (n_{PCDA} / n_{amine} , x_6) (Table S1 in the ESI). Linear multiple regression analysis suggests that the objective variable T_{trs} is represented using the explanatory variables by the following (eq. 1) with cross validation error (CVE) 15.75 °C. In the (eq. 1), the normalized coefficients indicate the relative weight of each explanatory variable.

$$y = 11.46x_1 - 31.37x_2 + 36.17x_3 - 1.835x_4 + 6.081x_5 + 8.483x_6 + 61.17 \dots \text{(eq. 1)}$$

The relationship between the predicted and measured T_{trs} was summarized in the true-error plot (Fig. 2c). The more plots near the diagonal line indicate the higher accuracy of the prediction model. We extracted the descriptors to prepare the sparse and simplified model. The M_w (x_2) and T_b (x_3) respectively have negative and positive coefficients with almost the same absolute values. The contribution of these factors is cancelled each other out. In addition, the coefficient of the L (x_4) smaller than that of the other factors can be ignored (Fig. S1 in the ESI). Therefore, the sparse prediction model was represented by the (eq. 2) using 3 descriptors, such as d_0 (x_1), m (x_5), and n_{PCDA} / n_{amine} (x_6), with cross validation error (CVE) 25.14 °C (Fig. 2d).

$$y = 13.11x_1 + 12.10x_5 + 5.390x_6 + 61.17 \dots \text{(eq. 2)}$$

According to the model, the T_{trs} can be roughly estimated from the descriptors d_0 , m , and $R_{PCDA/amine}$. Although the predicted T_{trs} is not so accurate, the model facilitates the design of the guests. The coefficients in (eq. 2) indicate that the T_{trs} has positive correlation with these three descriptors. The higher T_{trs} is achieved by the larger d_0 , m , and n_{PCDA} / n_{amine} . These descriptors are consistent with chemical relevance. The larger d_0 (x_1) implies that the stronger interaction is achieved between the guest molecules in the interlayer space. For example, the longer alkyl chains of the guest amine induce the stronger van der Waals interaction. The stronger interaction between the layer and guest is achieved on the layered composites with the larger m (x_5). Since the guest $C_n-(NH_2)_2$ ($m = 2$) coordinates with two host PCDA molecules, the mobility of the DA molecules is restricted by the guest amine. In contrast, the equimolar guest C_n-NH_2 ($m = 1$) and host PCDA molecules forms the more soft layered structure because of the interdigitated alkyl chains of the amine. As the n_{PCDA} / n_{amine} (x_6) increases, the more dense and rigid layered structure is formed. Therefore, the higher T_{trs}

is achieved by the larger d_0 , m , and n_{PCDA} / n_{amine} . If the flexible layered structures are prepared by the smaller d_0 , m , and n_{PCDA} / n_{amine} , the lower T_{trs} and responsivity to weaker friction force can be achieved. Here we chose PEI as the guest to achieve lower T_{trs} (Fig. 1b). The macromolecular amine is accommodated in the interlayer space with smaller d_0 . The low density of the imine group corresponds to smaller m and n_{PCDA} / n_{amine} . The soft layered polymer composites have potentials for responsivity to weaker external stimuli. In this manner, the sparse modeling facilitates to elucidate the specific factors related to the stimuli responsivity.

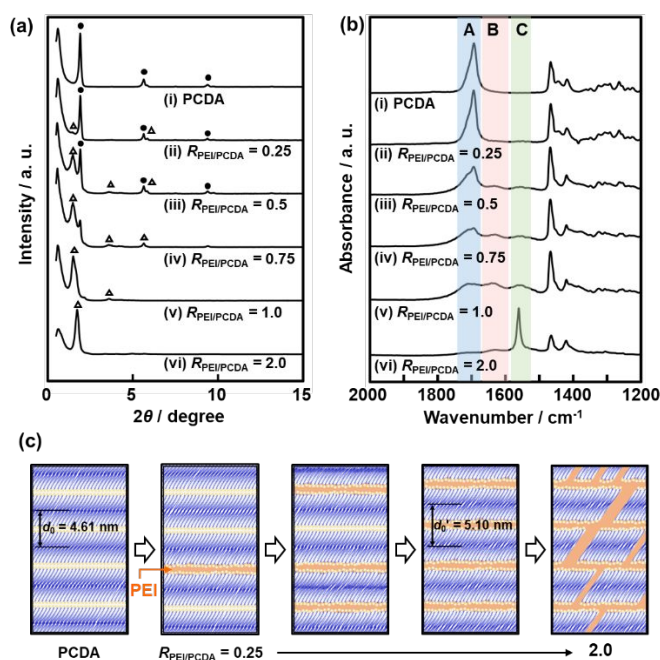


Fig. 3 Layered structures of PCDA and PCDA/PEI. (a) XRD patterns of PCDA (i) and PCDA/PEI at $R_{PEI/PCDA} = 0.25$ (ii), 0.5 (iii), 0.75 (iv), 1.0 (v), and 2.0 (vi). The filled circles and open triangles are assigned to the peaks corresponding to the original layered PCDA (d_0) and PCDA/PEI (d'_0), respectively. (b) FT-IR spectra of PCDA (i) and PCDA/PEI at $R_{PEI/PCDA} = 0.25$ (ii), 0.5 (iii), 0.75 (iv), 1.0 (v) and 2.0 (vi). (c) Schematic illustrations of the PCDA/PEI layered structures with an increase in the $R_{PEI/PCDA}$.

Soft layered polymer composites of PDA and PEI

The layered PDA/PEI was prepared by self-organization and topochemical polymerization. A commercial branched PEI ($M_n = 60,000$) was used as the guest (Fig. 1b). The precursor solution containing monomer PCDA and PEI was prepared with hexane. The molar ratio of PEI to PCDA ($R_{PEI/PCDA}$) was adjusted to $R_{PEI/PCDA} = 0.25, 0.5, 0.75, 1.0$, and 2.0 on the basis of the ethyleneimine monomer units. The weight content of PEI in the composite was calculated to be 2.79–18.7 wt% for $R_{PEI/PCDA} 0.25-2.0$. The layered composites of PCDA and PEI (PCDA/PEI) were obtained by evaporation of the solvent at room temperature under ambient pressure. The resultant PCDA/PEI was polymerized with irradiation of UV light. The detailed procedure was described in the ESI.

PCDA without the interlayer guest had the peaks at $2\theta = 1.91^\circ, 3.77^\circ$, and 5.65° corresponding to the lattice spacings 4.62 nm, 2.34 nm, and 1.56 nm, respectively (the circles in Fig. 3a). These peaks are assigned to d_0 / n ($n = 1, 2, 3$) of the layered

structure on the assumption of the interlayer distance (d_0) 4.62 nm (Fig. 3a). The peaks corresponding to additional interlayer distance (d_0') around 5.1–6.0 nm appeared with an increase in $R_{\text{PEI/PCDA}}$ (the triangles in Fig. 3a), whereas intensity of the original d_0 peaks was weakened. The peak corresponding to d_0' was only observed at $R_{\text{PEI/PCDA}} = 1.0$ and 2.0. The expanded interlayer distance (d_0') is comparable to $d_0 = 5.5$ nm and $d_0' = 5.2$ nm for accommodation of $\text{C}_4\text{H}_9\text{NH}_2$ and $\text{C}_3\text{H}_7\text{CH}(\text{NH}_2)\text{C}_3\text{H}_7$, respectively.⁶⁰ The facts indicate that the layered composites with the smaller interlayer distance and $n_{\text{PCDA}} / n_{\text{amine}}$ are obtained by accommodation of PEI.

The original PCDA showed the absorption band corresponding to the dimerized carboxy group around 1700 cm^{-1} on the Fourier-transform infrared (FT-IR) spectrum (the band A in Fig. 3b). As $R_{\text{PEI/PCDA}}$ increased, the peak of the dimerized carboxy group was broadened and weakened (Fig. 3b). On the other hand, the absorption peaks of the carboxylate and secondary amine groups were observed around $1580\text{--}1670\text{ cm}^{-1}$ and $1520\text{--}1580\text{ cm}^{-1}$, respectively (the bands B and C in Fig. 3b). These XRD and FT-IR analyses indicate that the PEI-intercalated PCDA domain is gradually increased with increasing $R_{\text{PEI/PCDA}}$ (Fig. 3c). The similar layered composites were obtained by a commercial linear PEI (Fig. S2 in the ESI). FT-IR analysis of the precursor solution suggests that the complex between the PCDA monomer and PEI is formed before evaporation of the solvent (Fig. S3 in the ESI). The complex is organized into the layered structure with evaporation of the solvent. The similar complexation and organization behavior were observed for PCDA and alkyl amines in our previous work.⁶⁰ In this manner, layered composites of PCDA/PEI were obtained from the precursor solution through self-organization with evaporation of the solvent.

Controlled stimuli-responsive color-change properties

After irradiation of UV-light, PDA/PEI was formed by the topochemical polymerization. The PDA/PEI powder showed the blue color characteristic to PDA derivatives (Fig. 4a and Fig. S4 in the ESI). The temperature-responsive color-change properties were studied to quantify the responsivity. The PDA and PDA/PEI showed the color change from blue to red with heating (Fig. 4a). The color-change temperature lowered with an increase in $R_{\text{PEI/PCDA}}$. This trend is consistent with the prediction model indicating the lower T_{trs} is achieved by the smaller $n_{\text{PCDA}} / n_{\text{amine}}$. The color-change behavior is characterized by the relationship between temperature (T) and x for the original PDA and PDA/PEI (Fig. 4b and Fig. S4 in the ESI). The T_{trs} , to achieve $0.5\Delta x$, was actually lowered from $60.8\text{ }^\circ\text{C}$ to $28.2\text{ }^\circ\text{C}$ with an increase in $R_{\text{PEI/PCDA}}$ from 0.25 to 2.0 (Fig. 4a,b and Fig. S4 in the ESI). The similar spectroscopic changes were observed on PDA and PDA/PEI at $R_{\text{PEI/PCDA}} = 2.0$ (Fig. S5 in the ESI). In our previous reports,^{53,60} the T_{trs} was changed in the range $39.2\text{--}106\text{ }^\circ\text{C}$ by the guest low-molecular-weight amines, such as alkyl amines and diamines, in the interlayer space. In the present work, the lower T_{trs} was achieved using PEI as the guest on the basis of the prediction. PEI contributes to formation of the more flexible layered structures compared with low

molecular-weight alkyl amines. These results imply that tuning of the stimuli responsivity can be achieved by the flexibility control of the layered PDA.

Differential scanning calorimetry (DSC) analysis indicates that the structure change of the layered PDA/PEI composites proceeds at lower temperature than that of pure layered PDA without guests. DSC thermogram of the pure layered PDA showed the endothermic peak around $65\text{ }^\circ\text{C}$ corresponding to deformation of the layered structure (the chart (i) in Fig. 4c).⁴⁰ This structure transition leads to the color change at T_{trs} through shortening the conjugation length of PDA main chain. The additional broadened endothermic peak appeared around $35\text{ }^\circ\text{C}$ at $R_{\text{PEI/PCDA}} = 0.25$ and 0.5 (the chart (ii) in Fig. 4c and Fig. S6 in the ESI). The endothermic peak around $35\text{ }^\circ\text{C}$ was only observed for the PDA/PEI at $R_{\text{PEI/PCDA}} = 0.75, 1.0$ and 2.0 (the chart (iii) in Fig. 4c). In contrast, pure branched PEI has not peak in this temperature range (Fig. S6 in the ESI). The DSC analysis supports the improved stimuli responsivity with the lower T_{trs} originates from the flexible layered structure of PDA/PEI. In addition, changes in the DSC thermograms imply the gradual formation of the flexible PDA/PEI domains with an increase in $R_{\text{PEI/PCDA}}$ (Fig. 3c).

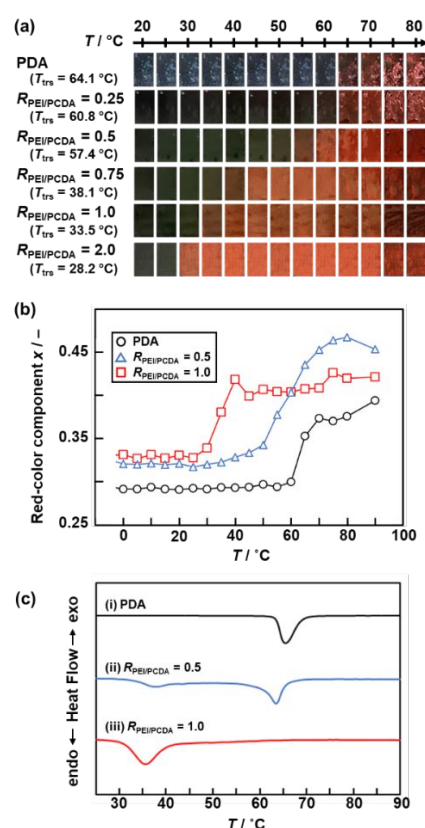


Fig. 4 Temperature-responsive color-change properties of PDA/PEI. (a) Photographs of the powdered samples with heating. (b) Relationship between T and x for PDA (circle) and PDA/PEI at $R_{\text{PEI/PCDA}} = 0.5$ (triangle) and 1.0 (square). (c) DSC thermograms of PDA (i) and PDA/PEI at $R_{\text{PEI/PCDA}} = 0.5$ (ii) and 1.0 (iii).

Paper-based device of the layered PDA/PEI

The PDA/PEI layered polymer composite was obtained as powder. The aggregates of the sheet-like PDA/PEI around $1\text{ }\mu\text{m}$

in width were observed by scanning electron microscopy (SEM) (Fig. S7 in the ESI). However, homogeneous friction force is not applied to the powdered state. Moreover, the paper-based device with homogenous coating and immobilization of the layered PDA/PEI is required to achieve the gradual color change in response to strength and number of the applied friction force (Fig. 5a). If the number of the color-changing domains from blue to red are increased on the cellulose fibers, the color of the paper-based device can be macroscopically changed by an increase in the number of applied friction force.

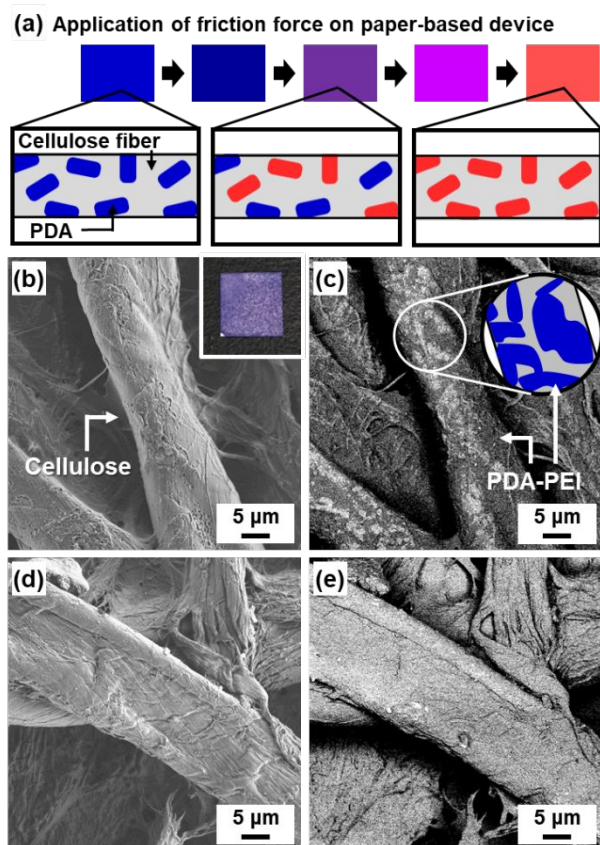


Fig. 5 Paper-based device with coating of PDA/PEI on a filter paper consisting of cellulose bundles. (a) Schematic models of color-changing properties with application of friction force on the paper-based device. The color of the device was changed with an increase in the number of the red domain. (b,c) Photograph (inset), SEM, and BSE images of PDA/PEI on a filter paper. (d,e) SEM and BSE images of a filter paper without coating as a reference.

Dip-coating was used to obtain the paper-based device with the homogenous coating. A filter paper was dipped in the precursor chloroform solution containing the monomer PCDA and PEI at $R_{PEI/PCDA} = 2.0$ around 5 sec. After evaporation of the solvent, topochemical polymerization was performed with irradiation of UV light. The PDA/PEI nanosheets were homogeneously coated on a filter paper (Fig. 5b–e). The PDA/PEI-coated paper showed the blue color (the inset of Fig. 5a). Although the deposited PDA/PEI was not clearly observed on the secondary electron (SE) image by scanning electron microscopy (SEM) (Fig. 5b), the black and white domains with clear contrast appeared on the back-scattered electron (BSE)

image (Fig. 5c). In general, contrast of the BSE image is generated from differences in composition and density.⁶⁹ Therefore, the black domains on the cellulose bundles correspond to the PDA/PEI-coated sheets (Fig. 5c). Although bundles of cellulose fibers were observed on a bare filter paper (Fig. 5d,e), the BSE image showed the homogeneous color without contrast (Fig. 5e). In this manner, the PDA/PEI was homogeneously coated on a filter paper. The coating density of the PDA/PEI was 0.56 mg cm^{-2} on a filter paper. The PDA/PEI-coated paper showed the same temperature-responsive color-change properties as those of the powdered samples (Fig. S8 in the ESI).

Measurement of weak friction force by the color

The designed PDA/PEI-coated paper-based device was applied to measure weak friction force (Fig. 6). The relationship between the friction force and color was studied to achieve the measurement. Friction force was applied to the PDA/PEI-coated paper by the probe at the bottom of a cage with weight (Fig. 6a and Fig. S9 in the ESI). The temperature of the paper-based device was kept at $20 \text{ }^\circ\text{C}$ using a temperature-controlled stage to avoid the color change by heat. The color of the PDA/PEI-coated paper was gradually changed from blue to red as the number of applied friction force (n_f) increased (Fig. 6a,b). The optical microscopy images indicate that the number of the red domain was gradually increased with an increase in n_f (Fig. 6c). The results mean that the number of the red-color PDA/PEI on the paper-based device was increased with increasing n_f . This color change was not caused by the friction heat. When the same friction force was applied to a commercial thermo-label on the same experimental setup, no color change originating from friction heat was observed (Fig. S10 in the ESI). The increment of the red-color intensity (Δx) was gradually raised with an increase in the n_f (Fig. 6d). The relationship between the n_f and Δx was obtained for four different strength of friction force (Fig. 6d). The four PDA/PEI-coated samples were used to measure Δx at each strength to ensure the reproducibility. The results indicate that the accumulated stress, i.e. n_f , is estimated from the Δx at the specific friction force. Moreover, unknown strength of friction force is quantified by the Δx at the constant n_f .

The standard curve was prepared for the quantitative detection of friction force (Fig. 6e). The friction force (F) was measured to be 0.20 N using a spring scale for the cage (109 g) without weight. When the weight 539 g , 1061 g , and 3000 g was loaded on the cage, the F was measured to be 1.20 N , 2.45 N , and 6.37 N , respectively (Fig. S9 in the ESI). The friction force was applied to the rectangular area L in length and d in width of the paper-based device with back-and-forth motion (Fig. 6a). Here the L and d are 5.0 mm and 0.76 mm , respectively. The number is defined as $n_f = n$ ($n = 0, 2, 4, 6, \dots, 20$). Therefore, the accumulated work (W / J) with the rubbing is calculated by the (eq. 3).

$$W = F \times L \times n_f \dots \text{(eq. 3)}$$

If the color change is assumed to be achieved homogeneously on the area L in length and d in width, the red-color intensity Δx is correlated to the W on the unit area by the (eq. 4), where k is a constant with unit $\text{mm}^2 \text{J}^{-1}$ ($= \text{mm} \text{N}^{-1}$). The constant k means to the responsibility of the device to the external stimulus.

$$\Delta x = k \frac{W}{d \times L} = k_d n_F \dots \text{(eq. 4)}$$

According to the (eq. 4), the Δx and $F d^{-1}$ have the linear relationship under the constant k and n_F . Here, $F d^{-1}$ ($\text{N} \text{mm}^{-1} = \text{J} \text{mm}^{-2}$) corresponds to the accumulated work on the unit area. The Δx at $n_F = 20$ was measured on each 12 samples for $F = 0.20 \text{ N}$, 1.20 N , and 2.45 N to ensure the reproducibility (the black filled circles in Fig. 6e). The average Δx had the linear relationship with the $F d^{-1}$ at $n_F = 20$. Therefore, unknown F can be estimated from Δx at $n_F = 20$ by (eq. 5) based on the linear approximation in Fig. 6e.

$$\Delta x = 2.64 \times 10^{-2} \times (F d^{-1}) - 8.52 \times 10^{-4} \dots \text{(eq. 5)}$$

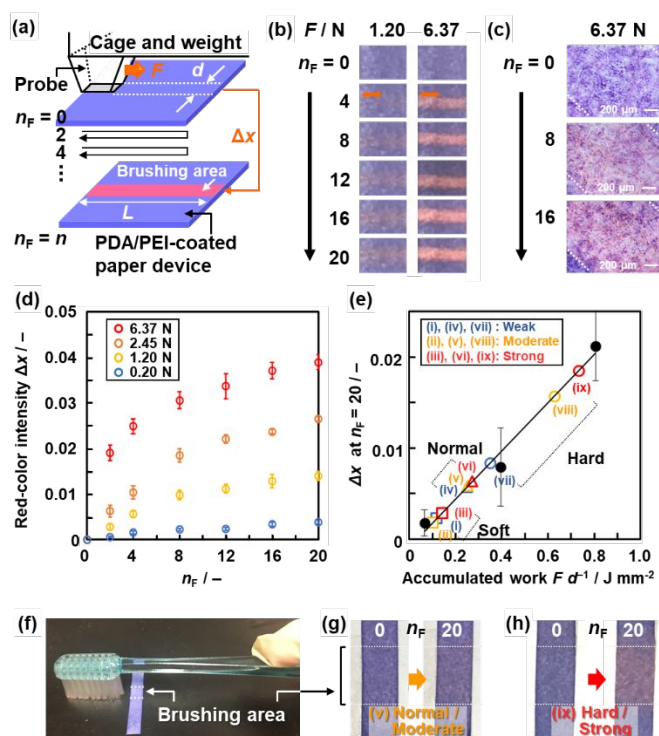


Fig. 6 Visualization and quantitative detection of friction force. (a) Schematic illustration of the experimental setup. (b) Color changes of the PDA/PEI-coated paper ($R_{\text{PEI/PCDA}} = 2.0$) with application of friction force 1.20 N and 6.37 N. (c) Optical microscopy images of the PEI/PDA-coated paper with application of friction force 6.37 N at $n_F = 0, 8$, and 16 . (d) Relationship between n_F and Δx with application of friction force at 0.20 N , 1.20 N , 2.45 N , and 6.37 N . (e) Relationship between the accumulated work ($F d^{-1}$) and x with application of friction force at 0.20 N , 1.20 N , 2.45 N under $n_F = 20$ as the standard curve for the quantification (the black plots). (f) Experimental setup for measurement of toothbrushing force. (g, h) Photographs before and after brushing by moderate strength using a normal brush (g) and strong strength using a hard brush (h). The colored plots (i)–(ix) in panel (e) represent the measured Δx values by different 9 combinations of brushing force and brush hardness, as listed in Table 1.

Application of the device to measurement of toothbrushing force

The paper-based device and measurement scheme are applied to estimate unknown weak friction force. Commercial toothbrushes with three different hardness, such as soft, normal, and hard, were used for quantification of brushing force on the PDA/PEI-coated paper (Fig. 6f). In general, appropriate brushing force is known to be $100\text{--}300 \text{ g}$ as weight when brush is pressed to a platform scale.^{27,28} The brushing test was performed by the same experimenter with three different strength measured by platform scale, such as weak for $50\text{--}100 \text{ g}$, moderate for $150\text{--}200 \text{ g}$, and strong for $250\text{--}300 \text{ g}$. The Δx at $n_F = 20$ was measured for the nine combinations of the different brushing force and hardness (Table 1). The measured Δx values were plotted in the standard curve (the colored plots in Fig. 6e). Then, F was estimated from the Δx by the (eq. 5), where the d of the toothbrush is 9.0 mm . The friction force F of toothbrushing was measured to be in the range of $0.91\text{--}6.60 \text{ N}$ (Table 1). The average friction force was 5.13 N for the hard brush, 2.33 N for the normal brush, and 1.08 N for the soft brush. The results imply that the brushing force mainly depends on the hardness of brush rather than the strength. Further study is needed to study the effects of the other factors, such as shape and composition of brushes and manual or electronic types. Understanding of brushing force contributes to keep our oral health.

Table 1 Friction force measured by different brushing force and brush hardness.

Hardness	Results	Brushing force		
		Weak	Moderate	Strong
Soft	$\Delta x / 10^{-3}$	2.29	1.81	2.89
	$F d^{-1} / \text{J} \text{mm}^{-2}$	(i) 0.119	(ii) 0.101	(iii) 0.142
	F / N	1.07	0.91	1.27
Normal	$\Delta x / 10^{-3}$	5.75	5.86	6.35
	$F d^{-1} / \text{J} \text{mm}^{-2}$	(iv) 0.250	(v) 0.254	(vi) 0.273
	F / N	2.25	2.29	2.45
Hard	$\Delta x / 10^{-3}$	8.40	15.7	18.5
	$F d^{-1} / \text{J} \text{mm}^{-2}$	(vii) 0.350	(viii) 0.628	(ix) 0.733
	F / N	3.15	5.65	6.60

Conclusions

Layered PDA and its paper-based device were designed and prepared for measurement of friction force. Sparse modeling, a data-scientific approach, assisted selection of the interlayer guest to achieve controlled stimuli-responsive color-changing properties. According to the prediction model, the guest PEI formed the more flexible layered structure exhibiting color changes with application of weaker external stimuli, such as low temperature and weaker friction force. The layered composites of PDA and PEI were homogeneously coated on a filter paper to induce the gradual color change in response to the number and

strength of the applied friction force. The red-color intensity was used for measurement of friction force. Therefore, unknown friction force was estimated from the color of the paper-based device. As a model case, toothbrushing force was colorimetrically measured using the PDA/PEI-coated paper. In general, it is not easy to achieve measurement of friction force by conventional materials and devices. The present paper-based device of the layered PDA with tunable responsivity has potentials for measurement of a wide range of friction force found in nature and daily life.

Conflicts of interest

There are no conflicts to declare.

Acknowledgements

This work was partially supported by JST PRESTO (Y.O., PMJPR16N2), Izumi Science and Technology Foundation (Y.O.), Asahi Glass Foundation (Y.O.).

Notes and references

- M. M. Caruso, D. A. Davis, Q. Shen, S. A. Odom, N. R. Sottos, S. R. White and J. S. Moore, *Chem. Rev.*, 2009, **109**, 5755.
- Y. Sagara and T. Kato, *Nat. Chem.*, 2009, **1**, 605.
- D. R. T. Roberts and S. J. Holder, *J. Mater. Chem.*, 2011, **21**, 8256.
- Y. Sagara, S. Yamane, M. Mitani, C. Weder, T. Kato, *Adv. Mater.*, 2016, **28**, 1073.
- C. Calvino, L. Neumann, C. Weder and S. Schretti, *J. Polym. Sci. Polym. Chem.*, 2017, **55**, 640.
- S. Stauss and I. Honma, *Bull. Chem. Soc. Jpn.*, 2018, **91**, 492
- R. Zhang, Q. Wang and X. Zhaeng, *J. Mater. Chem. C*, 2018, **6**, 3182.
- S. Hayashi, *Polymer J.*, 2019, **51**, 813.
- B. R. Crenshaw and C. Weder, *Chem. Mater.*, 2003, **15**, 4717.
- D. A. Davis, A. Hamilton, J. Yang, L. D. Cremer, D. V. Gough, S. L. Potisek, M. T. Ong, P. V. Braun, T. J. Martínez, S. R. White, J. S. Moore and N. R. Sottos, *Nature*, 2009, **459**, 68.
- K. Sakakibara, L. A. Joyce, T. Mori, T. Fujisawa, S. H. Shabbir, J. P. Hill, E. V. Anslyn and K. Ariga, *Angew. Chem. Int. Ed.*, 2012, **51**, 9643.
- H. Yuan, K. Wang, K. Yang, B. Liu and B. Zou, *J. Phys. Chem. Lett.*, 2014, **5**, 2968.
- S. Zeng, H. Sun, C. Park, M. Zhang, M. Zhu, M. Yan, N. Chov, E. Li, A. T. Smith, G. Xu, S. Li, Z. Hou, Y. Li, B. Wang, D. Zhang and L. Sun, *Mater. Horiz.*, 2019, DOI: 10.1039/c9mh00851a.
- Y. Gu, K. Wang, Y. Dai, G. Xiao, Y. Ma, Y. Qiao and B. Zou, *J. Phys. Chem. Lett.*, 2017, **8**, 4191.
- T. Kosuge, X. Zhu, V. M. Lau, D. Aoki, T. J. Martinez, J. S. Moore and H. Otsuka, *J. Am. Chem. Soc.*, 2019, **141**, 1898.
- Y. Sagara and T. Kato, *Angew. Chem. Int. Ed.*, 2008, **47**, 5175.
- H. Ito, M. Muromoto, S. Ishizaki, N. Kitamura, H. Sato and T. Seki, *Nat. Commun.*, 2013, **4**, 2009.
- K. Nagura, S. Saito, H. Yusa, H. Yamawaki, H. Fujihisa, H. Sato, Y. Shimoikeda and S. Yamaguchi, *J. Am. Chem. Soc.*, 2013, **135**, 10322.
- R. Yoshii, K. Suenaga, K. Tanaka and Y. Chujo, *Chem. Eur. J.*, 2015, **21**, 7231.
- L. Bai, P. Bose, Q. Gao, Y. Li, R. Ganguly and Y. Zhao, *J. Am. Chem. Soc.*, 2017, **139**, 1, 436.
- J. Zhao, Z. Chi, Y. Zhang, Z. Mao, Z. Yang, E. Ubba and Z. Chi, *J. Mater. Chem. C*, 2018, **6**, 6327.
- J. E. Sanders, B. S. Goldstein and D. F. Leotta, *J. Rehabil. Res. Dev.*, 1995, **32**, 214.
- E. McInnes, N. A. Cullum, S. E. M. Bell-Syer, J. C. Dumville and A. Jammali-Blasi, *Cochrane Database Syst. Rev.*, 2008, **4**, CD001735.
- S. Gogia and S. Neelamegham, *Biorehology*, 2015, **52**, 319.
- C. M. Fraleigh, J. H. Mc Elhaney and R. A. Heiser, *J. Dent. Res.*, 1967, **46**, 209.
- C. P. Turssi, A. B. Kelly and A. T. Hara, *J. Dent.*, 2019, **86**, 75.
- G. I. McCracken, J. Janssen, M. Swan, N. Steen, M. de Jager and P. A. Hesman, *J. Clin. Periodontol.*, 2003, **30**, 409.
- G. A. Van der Weijden, M. F. Tunmerman, E. Reijerse, C. M. Snoek and U. van der Velden, *J. Clin. Periodontol.*, 1996, **23**, 724.
- T. Ogawa, *Prog. Polym. Sci.*, 1995, **20**, 943.
- S. Okada, S. Peng, W. Spevak and D. Charych, *Acc. Chem. Res.*, 1998, **31**, 229.
- R. W. Carpick, D. Y. Sasaki, M. S. Marcus, M. A. Eriksson and A. R. Burns, *J. Phys. Condens. Matter.*, 2004, **16**, R679.
- M. A. Reppy and B. Piindzola, *Chem. Commun.*, 2007, 4317.
- D. J. Ahn and J. M. Kim, *Acc. Chem. Res.*, 2008, **41**, 805.
- D. J. Ahn, S. Lee and J. M. Kim, *Adv. Funct. Mater.*, 2009, **19**, 1483.
- X. Sun, T. Chen, S. Huang, L. Li and H. Peng, *Chem. Soc. Rev.*, 2010, **39**, 4244.
- R. Jelinek and M. Ritenberg, *RSC Adv.*, 2013, **3**, 21192.
- D. H. Park, B. J. Park and J. M. Kim, *Acc. Chem. Res.*, 2016, **49**, 1211.
- M. N. Tahir, A. Nyayachavadi, J. F. Morin and S. Rondeau-Gagne, *Polym. Chem.*, 2018, **9**, 3019.
- X. Qian and B. Städler, *Chem. Mater.*, 2019, **31**, 1196.
- M. Takeuchi, K. Gnanasekaran, H. Friedrich, H. Imai, N. A. J. M. Sommerdijk and Y. Oaki, *Adv. Funct. Mater.*, 2018, **28**, 1804906.
- S. Lee and J. M. Kim, *Macromolecules*, 2007, **40**, 9201.
- S. Dei, M. Matsumoto and A. Matsumoto, *Macromolecules*, 2008, **41**, 2467.
- S. Ampornpun, S. Montha, G. Tumcharern, V. Vchirawongkwin, M. Sukwattanasinitt, S. Wacharasindhu, *Macromolecules*, 2012, **45**, 9038.
- I. S. Park, H. J. Park and J. M. Kim, *ACS Appl. Mater. Interface*, 2013, **5**, 8805.
- I. S. Park, H. J. Park, W. Jeong, J. Nam, Y. Kang, K. Shin, H. Chung and J. M. Kim, *Macromolecules*, 2016, **49**, 1270.
- J. Huo, Q. Deng, T. Fan, G. He, X. Hu, X. Hong, H. Chen, S. Luo, Z. Wang and D. Chen, *Polym. Chem.*, 2017, **8**, 7436.
- W. Jeong, M. I. Khazi, D. G. Lee and J. M. Kim, *Macromolecules*, 2018, **51**, 10312.
- B. Hu, S. Sun, B. Wu and P. Wu, *Small*, 2019, **15**, 1804975.
- G. Shin, M. I. Khazi, U. Kundapur, B. Kim, Y. Kim, C. W. Lee and J. M. Kim, *Macromolecules*, 2019, **8**, 610.
- C. Khanantong, N. Charoenthai, F. Kielar, N. Traiphol and R. Traiphol, *Colloid Surfaces A*, 2019, **561**, 226.
- M. Okaniwa, Y. Oaki, S. Kaneko, K. Ishida, H. Maki and H. Imai, *Chem. Mater.*, 2015, **27**, 2627.
- M. Okaniwa, Y. Oaki and H. Imai, *Adv. Funct. Mater.*, 2016, **26**, 2463.
- Y. Ishijima, H. Imai and Y. Oaki, *Chem*, 2017, **3**, 509.
- M. Takeuchi, H. Imai and Y. Oaki, *ACS Appl. Mater. Interfaces*, 2017, **9**, 16546.
- M. Takeuchi, H. Imai and Y. Oaki, *J. Mater. Chem. C*, 2017, **5**, 8250.
- Y. Oaki, Y. Ishijima and H. Imai, *Polym. J.*, 2018, **50**, 319.
- T. Kato, J. Uchida, T. Ichikawa and T. Sakamoto, *Angew. Chem. Int. Ed.*, 2018, **57**, 4355.

- 58 K. Ariga, S. Watanabe, T. Mori and J. Takeya, *NPG Asia Mater.*, 2018, **10**, 90.
- 59 P. Ganter, L. M. Schoop and B. V. Lotsch, *Adv. Mater.*, 2017, **29**, 1604884.
- 60 H. Terada, H. Imai and Y. Oaki, *Adv. Mater.*, 2018, **30**, 1801121.
- 61 K. Fujimura, A. Seko, Y. Koyama, A. Kuwabara, I. Kishida, K. Shitara, C. A. J. Fisher, H. Moriwake and I. Tanaka, *Adv. Energy Mater.*, 2013, **3**, 980.
- 62 K. Sodeyama, Y. Igarashi, T. Nakayama, Y. Tateyama and M. Okada, *Phys. Chem. Chem. Phys.*, 2018, **20**, 22585.
- 63 J. S. Peerless, N. J. B. Milliken, T. J. Oweida, M. D. Manning and Y. G. Yingling, *Adv. Theory Simul.*, 2019, **2**, 1800129.
- 64 S. A. Tawfik, O. Isayev, C. Stampfl, J. Shapter, D. A. Winkler and M. J. Ford, *Adv. Theory Simul.*, 2019, **2**, 1800128.
- 65 G. Nakada, Y. Igarashi, H. Imai and Y. Oaki, *Adv. Theory Simul.*, 2019, **2**, 1800180.
- 66 R. Tibshirani, M. Wainwright and T. Hastie, *Statistical Learning with Sparsity: The Lasso and Generalizations*; Chapman and Hall/CRC: Philadelphia, PA, 2015.
- 67 Y. Igarashi, H. Takenaka, Y. Nakanishi-Ohno, M. Uemura, S. Ikeda and M. Okada, *J. Phys. Soc. Jpn.*, 2018, **87**, 044802.
- 68 E. Reinhard, W. Heidrich, P. Debevec, S. Pattanaik, G. Ward and K. Myszkowski, *High Dynamic Range Imaging: Acquisition, Display, and Image-Based Lighting*, Elsevier Science, Saint Louis, 2nd edn, 2010, ch. 2, p. 35.
- 69 K. Shimizu and T. Mitani, *New Horizons of Applied Scanning Electron Microscopy*, Springer Series in Surface Sciences 45, 2009.

Graphical Abstract

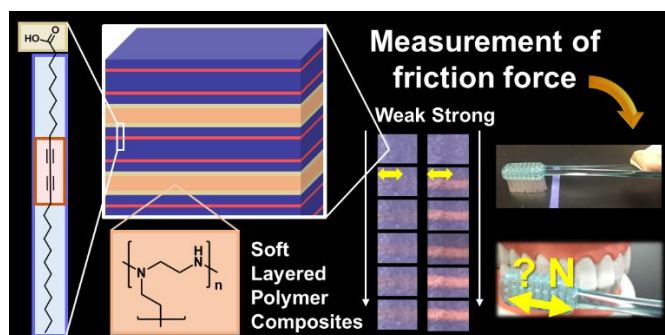
Paper-based device of designer soft layered polymer composites for measurement of weak friction force

Kei Watanabe,^a Hiroaki Imai,^a Yuya Oaki*,^{a,b}

^a Department of Applied Chemistry, Faculty of Science and Technology, Keio University, 3-14-1 Hiyoshi, Kohoku-ku, Yokohama 223-8522, Japan

^b JST, PRESTO, 4-1-8 Honcho, Kawaguchi 332-0012, Japan

Email oakiyuya@aplc.keio.ac.jp



The paper-based device of designer soft layered composite consisting of polydiacetylene enables measurement of friction force with gradual color change from blue to red in response to the strength and number of the applied friction force.

